

## ARTICLE OPEN

## Role of synoptic activity on projected changes in upwelling-favourable winds at the ocean's eastern boundaries

Catalina Aguirre<sup>1,2,3\*</sup>, Maisa Rojas<sup>1,4</sup>, René D. Garreaud<sup>1,4</sup> and David A. Rahn<sup>5</sup>

The climate of the ocean's eastern boundaries is strongly influenced by subtropical anticyclones, which drive a surface wind stress that promotes coastal upwelling of nutrient-rich subsurface water that supports high primary productivity and an abundance of food resources. Understanding the projected response of upwelling-favourable winds to climate change has broad implications for coastal biogeochemistry, ecology, and fisheries. Here we use a reanalysis, an ensemble of global climate simulations, and an objective algorithm to track anticyclones to investigate the projected changes in upwelling-favourable wind events at the California, Canary, Humboldt, and Benguela coastal upwelling systems. Except for the north Pacific, we find consistent poleward shifts of mean and upper percentile daily winds over the ocean basins. We propose that extratropical, synoptic-scale migratory anticyclones that force intense coastal upwelling events—which become more frequent at higher latitudes and less frequent at lower latitudes in the future—play an important role in the projected changes in upwelling-favourable wind events in these coastal upwelling systems. These changes complement large-scale processes such as the poleward shift of the subtropical ridge (STR) and stationary subtropical highs. Hence, both extratropical and tropical processes need to be considered to fully explain projected changes at the coastal upwelling systems under anthropogenic climate change.

*npj Climate and Atmospheric Science* (2019)2:44; <https://doi.org/10.1038/s41612-019-0101-9>

## INTRODUCTION

Subtropical anticyclones are important features that influence the climate of the ocean eastern boundaries. These high-pressure systems drive predominately alongshore equatorward winds<sup>1</sup> (Fig. 1). The resulting wind stress field promotes coastal upwelling of salty, cool, oxygen-poor, and nutrient-rich subsurface waters. Ample nutrients support high primary productivity and an abundance of fishery resources that impact the economy of adjacent countries at the Humboldt, Benguela, California, and Canary Eastern Boundaries Upwelling Systems (EBUS). Thus, projecting the response of upwelling-favourable winds to climate change is of particular relevance given the broad implications for coastal biogeochemistry, ecology, and fisheries.<sup>2–5</sup>

Previous studies have investigated projected changes in EBUS under warming climate scenarios using an ensemble of ocean–atmosphere coupled models. They show that changes of surface winds in a warmer climate will result in an increase of the summer mean upwelling-favourable winds at the poleward portions of the present-day EBUS<sup>6,7</sup> (except in the California system). Two physical mechanisms have been proposed to explain those changes. The first is Bakun's hypothesis<sup>6</sup> in which the temperature contrast between the land and ocean enhances the cross-shore thermal gradient and thus the low-level pressure gradient. Nevertheless, the increased land–ocean temperature differences are ubiquitous in projections of future conditions, while the increase in upwelling-favourable winds is limited to the poleward portion of the upwelling region. The latitudinal pattern of changes in upwelling-favourable winds along the EBUS is more consistent with a poleward displacement of the subtropical anticyclones and not Bakun's hypothesis.<sup>7</sup> These previous studies have focused on changes of the summer mean (or median) upwelling, but not on the change in the full distribution of daily

wind. For the Humboldt system, a single model was used to analyse changes in upwelling-favourable winds in a warmer climate and interpreted through changes in the full distribution. The results indicated that there were fewer weak events and more moderate to intense events without a significant change in the extremes.<sup>3</sup>

At synoptic time scales, the equatorward winds along the EBUS exhibit periods of intensification that typically last 2–5 days and are interrupted by periods of relaxed winds.<sup>9</sup> The strong wind stress on the ocean surface forces upward vertical velocities in the ocean near the coast through Ekman transport and Ekman pumping.<sup>10,11</sup> These short lived but intense upwelling-favourable wind events result in coastal cooling, intensified surface currents, and low values of dissolved oxygen and pH,<sup>12–15</sup> as well as impacts on lower trophic level dynamics and recruitment of different species.<sup>16,17</sup> Thus, an analysis of climate change projections of synoptic-scale upwelling-favourable wind events is essential to foresee the most likely environmental changes along EBUS.

Here we use an ensemble of simulations of the historical and the RCP8.5 scenario from the Coupled Model Intercomparison Project Phase 5 (CMIP5) to investigate the projected changes of upwelling-favourable wind stress (used as a proxy for upwelling) for the four EBUS during summer, considering both changes in central values and extreme events. Changes in synoptic upwelling-favourable wind events are diagnosed by quantifying variations in the upper part of the wind probability distributions, relating them to projected changes in migratory anticyclones at mid-latitudes.

## RESULTS

To provide a global context, Fig. 1 depicts the climatological Subtropical Anticyclones that exist west of the four EBUS and the

<sup>1</sup>Centro de Ciencia del Clima y la Resiliencia, CR2, Santiago, Chile. <sup>2</sup>Escuela de Ingeniería Civil Oceánica, Facultad de Ingeniería, Universidad de Valparaíso, Valparaíso, Chile.

<sup>3</sup>Centro de Observación Marino para estudios de Riesgos del ambiente costero, COSTAR, Valparaíso, Chile. <sup>4</sup>Departamento de Geofísica, Facultad de Ciencias Físicas y Matemáticas, Universidad de Chile, Santiago, Chile. <sup>5</sup>Department of Geography and Atmospheric Science, University of Kansas, Lawrence, KS, USA. \*email: catalina.aguirre@uv.cl

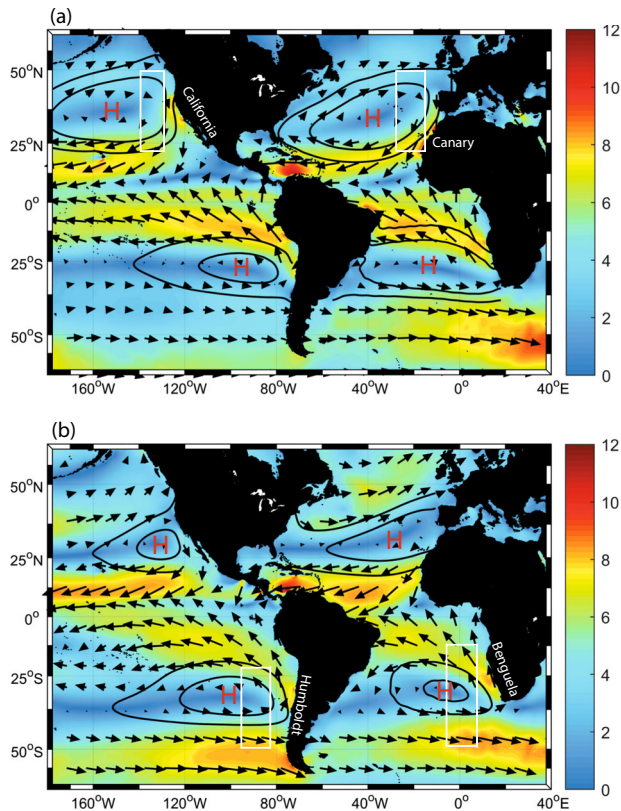


**Fig. 1** Subtropical highs and surface winds at the Eastern Boundary Upwelling Systems. CSFR reanalysis climatological 10-m winds (vectors) and magnitude (colours,  $\text{ms}^{-1}$ ) for the period 1979–2010: **a** June–July–August mean, **b** December–January–February mean. Black contours correspond to 1020 hPa and 1017 hPa sea-level pressure, indicating the position of the climatological subtropical anticyclones. White boxes indicate the regions considered to find migratory anticyclones offshore the four coastal upwelling regions.

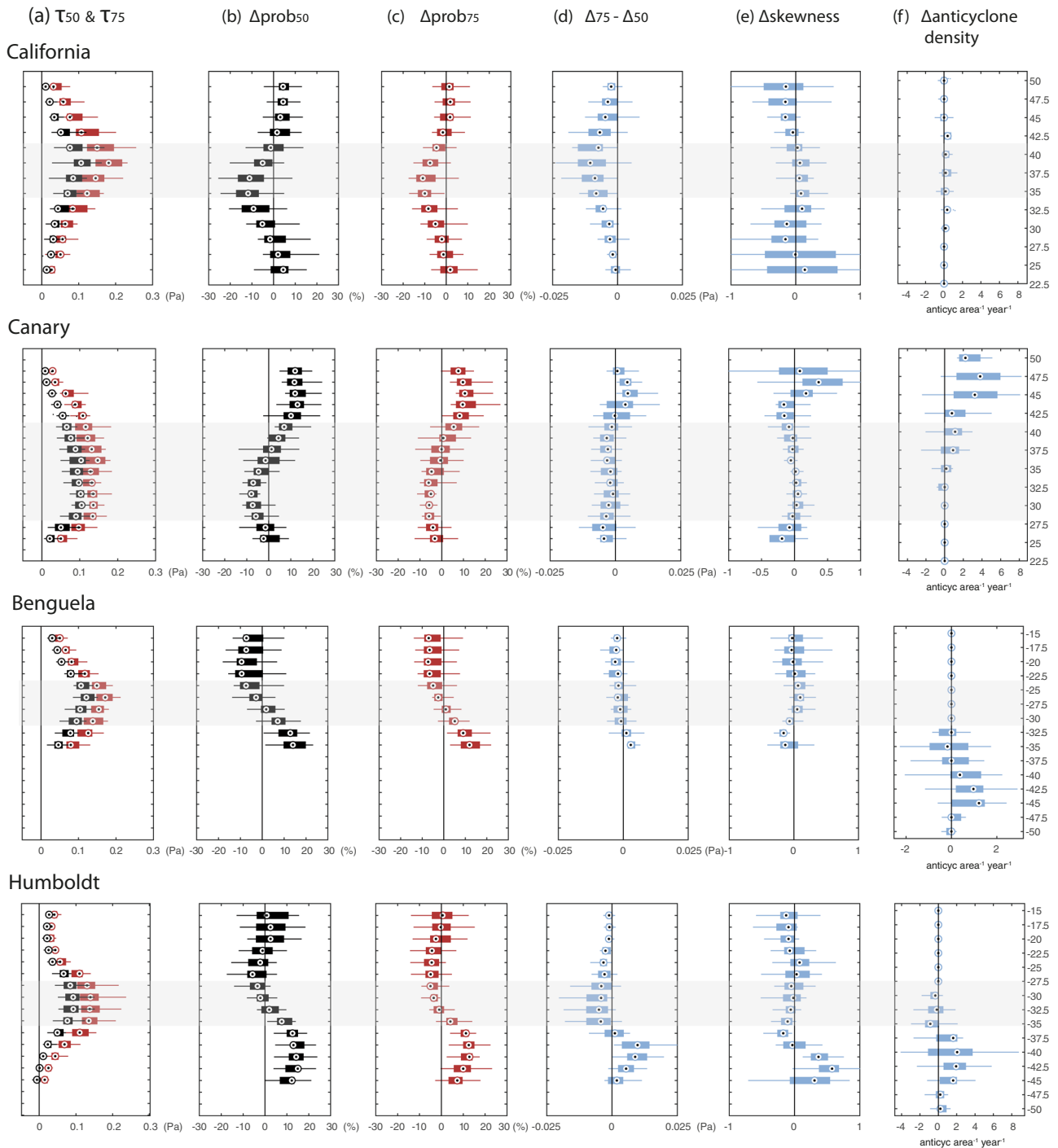
associated 10-m wind vectors and magnitudes. During June–July–August (JJA), subtropical anticyclones extend over the Northern Atlantic and Pacific Ocean basins with clear maxima in wind speed along their eastern flank. During December–January–February (DJF), the Northern Hemisphere (NH) subtropical anticyclones become weak and winds on their eastern flank relax. In the Southern Hemisphere (SH), the subtropical surface pressure increases at the end of austral winter, which corresponds to the strongest intensity of the Hadley cell. The peak zonal asymmetry of the subtropical anticyclones in the Southern Hemisphere occurs during austral spring and summer.<sup>18</sup> In both hemispheres, the equatorward, upwelling-favourable surface flow along the eastern flank of the subtropical anticyclones have average speeds of  $7\text{--}9\text{ m s}^{-1}$  during their corresponding summer season. In contrast, the alongshore winds during winter have average speeds lower than  $4\text{ m s}^{-1}$  and may be even downwelling-favourable.

Figure 2a (leftmost column) shows the model distributions of the summer wind stress corresponding to the 50th and 75th percentile ( $\tau_{50}$ ,  $\tau_{75}$ ) in the historical simulations as a function of latitude along the coast of each EBUS region. Figure 2b, c depicts the probability difference between the future (2080–2100) and present-day (1970–1990) daily alongshore wind stress for the median ( $\Delta\text{prob}_{50}$ ) and the upper-portion of the distribution ( $\Delta\text{prob}_{75}$ ). A graphical example of the method for this calculation can be found in Supplementary Fig. 1 for a particular model (see Methods). Changes observed in the median are consistent with previous work<sup>6,7</sup> and show an increase in summer upwelling-

favourable winds in the poleward portions of Humboldt, Benguela, and Canary, and a decrease in the California System. For Humboldt, Benguela, and Canary, the largest changes in strong events ( $\tau_{75}$ ) are observed poleward of the present-day core upwelling region (i.e. the latitudes where the present-day wind stress is greatest, grey horizontal bands in Fig. 2), where strong events of upwelling will increase between 5% and 20% as compared to the present climate. At the core of upwelling region, little change in the occurrence of intense wind events or even a slight decrease is projected. California exhibits a completely different pattern with the intense wind events decreasing in the core upwelling region ( $\sim 30\text{--}40^\circ\text{N}$ ) and no clear signal elsewhere. The probability difference of both the 50th and 75th percentile ( $\Delta\text{prob}_{50}$ ,  $\Delta\text{prob}_{75}$ ) shows a similar spatial pattern in the four eastern boundaries (Fig. 2b, c). To evaluate changes in intense events with respect to changes in the median and to focus on changes in the shape of the wind stress distribution, we calculated changes in the skewness and in the values of wind stress at the 50th and 75th percentile ( $\Delta_{50}$ ,  $\Delta_{75}$ ) between the present and future periods (Fig. 2d, e). A positive (negative) difference indicates that extreme events are increasing (decreasing) more (less) than the median.

In Canary, Humboldt, and Benguela, positive values of  $\Delta_{75} - \Delta_{50}$  are found at the poleward side of the core upwelling system. Conversely, negative values of  $\Delta_{75} - \Delta_{50}$  are found at the present-day core upwelling region in the California system (Fig. 2d). Changes in skewness indicate a change in the tail of the wind stress distribution (Fig. 2e). The positive change of skewness observed at the poleward portions of the Humboldt and Canary system indicates that in the future the wind stress distribution will include more frequent occurrences of extreme events at these latitudes. No clear and robust change in skewness is found for California nor Benguela, where future changes in wind stress are due to a shift in the position of the median in the probability distribution and not its shape.

We propose that the increase in strong upwelling events is linked to an augmented passage of migratory anticyclones. Such a link is observed in the present day climate, when upwelling events at a given latitude are forced by an enhanced pressure gradient that is associated with the passage of a surface anticyclone.<sup>19</sup> To support this hypothesis, we calculated the present-day probability that an upwelling-favourable wind stress above the 75th percentile occurs along an eastern boundary when a migratory anticyclone (identified by the tracking algorithm) resides inside the boxes shown in Fig. 1. Reanalysis data show that when a migratory anticyclone approaches the coast there is a high probability ( $\sim 75\%$ ) that an intense upwelling-favourable wind event occurs along the eastern boundary (Fig. 3), similar results are found when repeating this calculation with models. For the Humboldt system, the calculation with models indicates that the probability is even higher in present-day simulations with values between 75% and 100%. In Benguela, California, and Canary systems, the probability of a strong, upwelling-favourable wind day when a migratory anticyclone is offshore is  $\sim 60\text{--}70\%$ . Off California, the probability of high wind associated with a migratory anticyclone has a larger spread amongst the models. In general, little change is observed in the relationship between a migratory anticyclone and intense upwelling winds in the future climate in Benguela, California, and Canary. Unlike these coastal systems, in Humboldt the probability of strong wind in the presence of a migratory anticyclone decreases in the future ( $\sim 70\%$ ). To refine the relationship, a similar analysis was repeated for the present climate but at different latitudes (Supplementary Fig. 2). Due to fine-scale details, including the representation of the coastline and topography that varies among models, the overall relationship between a migratory anticyclone and an intense wind stress event at a particular latitude is less significant.



**Fig. 2** Projected changes in upwelling-favourable wind stress and migratory anticyclones by latitude. **a** Wind stress values at 50th (black boxes,  $T_{50}$ ) and 75th (red boxes,  $T_{75}$ ) percentiles of the historical simulations in the period 1970–1990. **b** Difference in the probability of occurrence of the wind stress value of 50th percentile between the future (2080–20100) and the present day (1970–1990) distributions (see Supplementary Fig. 1a). **c** Difference in the probability of occurrence of the wind stress value of 75th percentile between the future (2080–2100) and the present-day (1970–1990) distributions (see Supplementary Fig. 1b). **d** Difference ( $\Delta_{75} - \Delta_{50}$ ) of the changes of wind stress values of 50th ( $\Delta_{50}$ ) and 75th ( $\Delta_{75}$ ) between present (1970–1990) and future (2080–2100). **e** Difference in skewness of the wind stress distribution between future (2080–2100) and present (1970–1990). **f** Difference in the density of migratory anticyclones between future (2080–2100) and the present (1970–1990) off the coastal upwelling regions. Circle indicates median, boxes the range 25th and 75th percentiles, and lines extend to the most extreme data points of the 16 models. Dots are outliers. The grey horizontal bands indicate the location of strongest wind stress in the historical simulations during the period 1970–1990.

Included in Fig. 2f is the future-minus-present difference in migratory anticyclone density at the eastern boundaries. The spatial pattern of increased anticyclone activity is consistent with the differences in the frequency of intense wind events. In

Humboldt, Benguela, and Canary, an increase in migratory anticyclone density occurs at the poleward boundary of the core region of the upwelling system or at higher latitudes in the case of Benguela where the boundary of the African continent limits



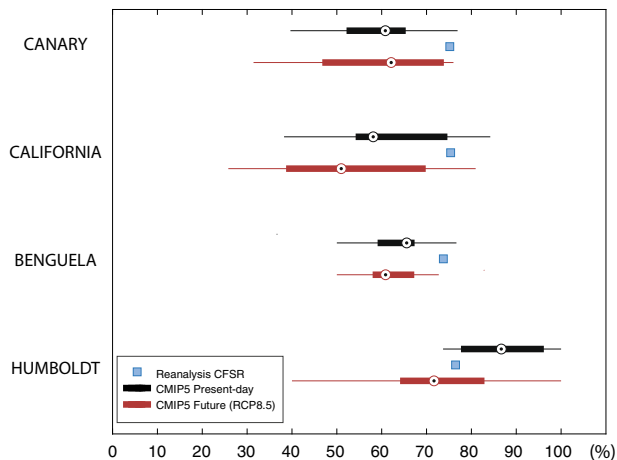


**Fig. 3** Relationship between migratory anticyclones and intense upwelling winds. Probability that a wind stress greater than the 75th percentile occurs together with a migratory anticyclone inside of the boxes defined in Fig. 1, for reanalysis CFSR and models for historical period (1970–1990) and projections under the RCP8.5 scenario (2080–2100). Circle indicates median, boxes the range 25th and 75th percentiles, and lines extend to the most extreme data points of the 16 models.

changes in upwelling-favourable winds. In contrast, no clear signal emerges in the north Pacific and there is more dispersion among the models. The future increase in the migratory anticyclone density at the poleward portion of the Humboldt system seems to be contradictory with the decrease in the probability of strong wind in the presence of a migratory anticyclone. This is likely due to the substantial reduction of the Andes height and steepness south of  $\sim 42^{\circ}\text{S}$ , which is also where the coastline becomes more irregular. So, if the anticyclones migrate southward in the future, they will encounter a much less pronounced coastal topography that is an important factor that promotes the development of intense wind events in this coastal boundary.<sup>19,20</sup>

To provide a large-scale picture of the circulation changes, Fig. 4 shows the difference between the future and present-day stationary and migratory anticyclone density for the whole globe. Included in the figure is the latitude of the maximum sea-level pressure (SLP) and the position of the subtropical ridge (STR). Most of the tracked anticyclones are stationary and conform to the semi-permanent nature of the subtropical anticyclones. Eastward propagating migratory anticyclone disturbances represent about 8% and 10% of the total number of anticyclones found by the tracking system in the NH and SH, respectively (Supplementary Fig. 3). There is a clear poleward shift in anticyclone tracks in the SH and in the North Atlantic (Fig. 4), including a poleward shift of the STR, which is a robust result offshore Humboldt, Benguela, and Canary. The STR of the present climate is located around  $34^{\circ}\text{S}$  off the coast of Humboldt and Benguela and a poleward displacement of  $2^{\circ}$  is projected for the future. Near Canary, the STR is found at  $42^{\circ}\text{N}$  in the present climate and is shifted  $1^{\circ}$  poleward in the future climate (Fig. 4a). In California, there is a poleward shift of the stationary anticyclone density, but neither the migratory subtropical anticyclones nor the STR is projected to change significantly. The shift in the density of disturbances in the SH is much clearer and more well-defined than in the NH. This agrees with previous results that show a more concentrated belt of anticyclones in the SH and a less-defined belt in the NH.<sup>21</sup> In the NH, the pattern for the Atlantic basin is also a poleward shift of these migratory anticyclones.

## DISCUSSION

Climate change projections indicate a poleward shift of stationary anticyclones at subtropical latitudes.<sup>7</sup> A poleward shift of subtropical anticyclones explains the strengthening (weakening) of mean upwelling-favourable winds at high (low) latitudes of the upwelling systems.<sup>22</sup> This poleward migration is also consistent with changes in the large-scale tropical atmospheric circulation, including an expansion of the Hadley cell under global warming<sup>23</sup> and an intensification of the subtropical highs.<sup>24</sup> In addition, this poleward expansion of the tropical atmospheric processes has already been observed in recent decades for different EBUS systems.<sup>25,26</sup>

In this work, we also found a future poleward shift in the density of migratory anticyclones in the North Atlantic and at all longitudes in the Southern Hemisphere. In the Canary, Humboldt, and Benguela systems, these shifts contribute to the increase in short-lived but strong upwelling-favourable wind events poleward of where the present-day alongshore wind maximum occurs, and hence provide a key mechanism for projected changes in upwelling-favourable winds at EBUS. A recent study of long-term anticyclone activity using reanalysis data (without the distinction between stationary and migratory anticyclones) shows that anticyclone variability is associated with the Southern Annular Mode (SAM) in the Southern Hemisphere and the Arctic Oscillation (AO) in the Northern Hemisphere.<sup>21</sup> Furthermore, the strongest trend over recent decades in anticyclone activity has been observed in the Southern Hemisphere, including increases in anticyclone frequency in the mid-latitudes and decreases for adjacent latitudes, which are partially attributed to changes in SAM during summer.<sup>21</sup> This spatial pattern is similar to the differences we found between projections and historical simulations, suggesting that projected latitudinal changes in migratory anticyclone density would be related to positive trends of SAM and AO in climate projections.<sup>27,28</sup> Furthermore, the poleward shift in the density of migratory anticyclones is consistent with a poleward shift of extratropical cyclone tracks,<sup>29</sup> since the hemispheric belts of migratory anticyclones are located equatorward of the main mid-latitude storm tracks.<sup>21</sup>

It is important to note that the equatorward coastal wind along the EBUS can intensify and manifest as a coastal low-level jet (LLJ).<sup>30</sup> LLJs occur year-round but are more frequent and intense during the summer.<sup>9,31–33</sup> Various climate studies of LLJs have been performed for the present climate,<sup>30,33,34</sup> but projections of the responses of LLJs to climate change are still limited.<sup>35,36</sup> Although LLJs are fine-scale phenomena and depend on processes not resolved in coarser-resolution global circulation models such as mesoscale responses to variations of the coastline and topography, our results concerning changes in intense wind events and the poleward shift of migratory anticyclones suggest that the LLJs will also shift poleward in the Canary<sup>36</sup> and Humboldt systems, since the presence of an anticyclone has been recognized as the main ingredient for the development of a LLJ. We acknowledge that biases exist in the nearshore wind fields and that modification of the mesoscale features of the wind near the coast is lacking in the coarse General Circulation Models (GCMs).<sup>37</sup> However, we highlight that the relative changes in synoptic patterns that force high-wind events are indeed represented in GCMs.

Near California, the summer trends of coastal winds only depict a decrease of upwelling between  $\sim 30$  and  $40^{\circ}\text{N}$  with no clear signal elsewhere. This is consistent with previous works that show future decreases in summertime wind stress in the California system. However, models project upwelling intensification during April and May at a portion of the central and northern California coastline.<sup>7,38</sup> Furthermore, the California region also demonstrates a more diffuse belt of anticyclones and a large variability of the relationship between high-wind events and migratory

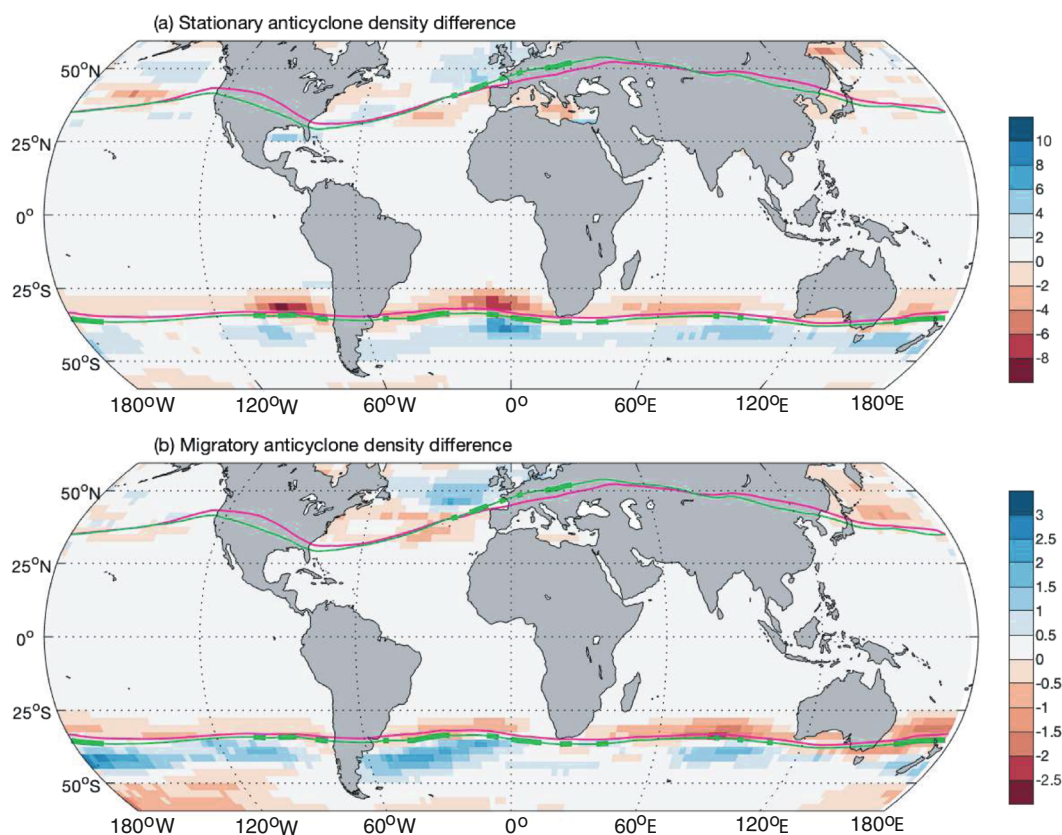


**Fig. 4** Projected changes in anticyclone density. CMIP5 ensemble mean difference of anticyclone density between periods 2080–2100 and 1970–1990. Colours: anticyclone density difference (anticycl area<sup>-1</sup> year<sup>-1</sup>), for summer in respective hemisphere. **a** Stationary anticyclones, **b** migratory anticyclones. Magenta line: position of the subtropical ridge for the period 1970–1990, green line: position of the subtropical ridge for the period 2080–2100. Green line is thick where at least 70% of the models exhibit a poleward position of the subtropical ridge in the future.

anticyclones amongst the 16 models, which also contributes to more ambiguous results.

In summary, three of the four main EBUS of the world will experience a substantial increase in the occurrence of short-lived but strong upwelling-favourable wind events, superimposed on a general increase in the seasonal mean alongshore wind. Both changes (mean and intense events) are caused by an overall poleward shift of the large-scale climatological circulation features in the Southern Hemisphere, and to a lesser extent in the Northern Hemisphere, including stationary subtropical anticyclones and migratory anticyclones along the mid-latitudes.

Finally, this study analyses changes in upwelling-favourable winds in EBUS, but not upwelling directly, and hence not the direct impact to marine life. Other variables, such as ocean stratification<sup>39</sup> for example, need to be considered in order to resolve the dynamics of upwelling in a warming climate and assess its ecological and socioeconomic impacts.

## METHODS

Daily and monthly SLP and 10-m winds were obtained from the Climate Forecast System Reanalysis (CFSR)<sup>40</sup> and from 16 CMIP5 model simulations using the historical (1970–2005) and the RCP8.5 scenario (2006–2100) experiments (Supplementary Table 1). Compared to the total set of Representative Concentration Pathways (RCPs), the RCP8.5 scenario corresponds to the pathway with the highest greenhouse gas emissions and is named according to the equivalent effect in the radiative forcing in the year 2100, relative to preindustrial period (i.e. +8.5 W m<sup>-2</sup>).<sup>41</sup> When

more than one simulation existed for a given experiment, only the first ensemble member (r1i1p1) was considered.

Given the nonuniform model resolution in CMIP5, each model's landmask and wind data were extracted and only the wind from grid points over the ocean were used to interpolate to a standard 1°×1° horizontal grid. The interpolated 10-m wind is then used to calculate the alongshore wind with respect to the adjacent coastal direction following the angles defined in Wang et al.<sup>6</sup> These alongshore winds are defined as “upwelling-favourable winds” when directed equatorward. We calculate alongshore wind stress based on Smith<sup>42</sup> from daily 10-m wind data using the air–sea package developed by Rich Pawlowicz and Bob Beardsley (available at <https://www.usgs.gov/software/sea-mat-matlab-tools-oceanographic-analysis>) with a constant air temperature of 10 °C. Here, the wind stress is used as a proxy for the actual coastal upwelling through Ekman transport.<sup>6</sup> Note, however, that coastal upwelling could also be modified by curl-driven processes via Ekman pumping<sup>11,43</sup> and by other processes such as changes to thermal stratification or remote ocean forcing.<sup>39</sup>

Throughout the whole study, we focus on the summer season, JJA for the Northern Hemisphere and DJF for the Southern Hemisphere. Changes to the spring onset of the upwelling season can have important phenological impacts,<sup>44</sup> but we are limiting this study to only the summer months following previous research that examine changes in upwelling systems using CMIP5 data.<sup>5,7</sup>

Our approach to investigate the changes of intense alongshore wind stress considers changes of the median (50th) and the upper quartile (75th) of the daily wind stress distributions. To consider changes in the upwelling events, we construct the cumulative frequency distribution for the period 1970–1990 (adopted here as the baseline for present-day climate) and for the period 2080–2100 of the RCP8.5 scenario at the near-coastal points along the upwelling systems. Supplementary Fig. 1

illustrates how the difference of probability of 50th and 75th percentiles ( $\Delta\text{prob}_{50}$  and  $\Delta\text{prob}_{75}$ , respectively) are obtained. Supplementary Fig. 1 also shows the differences between the future and present-day wind stress values for the 50th percentile ( $\Delta_{50}$ ) and 75th percentile ( $\Delta_{75}$ ). This method is applied to all 16 models and results are presented as the distribution of probability obtained from the different simulations, where circles indicate the median, boxes indicate the range of the 25th and 75th percentiles, and the lines extend to the most extreme data points. Outliers (dots) are defined as greater than  $q_3 + 1.5 (q_3 - q_1)$  or less than  $q_1 - 1.5 (q_3 - q_1)$ , where  $q_1$  and  $q_3$  are the 25th and 75th percentiles of the sample data, respectively.

Daily SLP is interpolated onto a  $2.5^\circ \times 2.5^\circ$  horizontal grid and used as input to a cyclone-tracking scheme developed and implemented at the University of Melbourne.<sup>45</sup> This method has been widely used for tracking both cyclones and anticyclones.<sup>21,46</sup> We locate and track high-pressure systems. From the total number of anticyclones identified, we separate stationary and migratory anticyclones. Migratory anticyclones are defined as anticyclones that last at least 3 days and move eastward faster than about  $3^\circ/\text{day}$ . The cyclone-tracking scheme was run for all 16 models for the summer months in each hemisphere and for the two analysis periods. Monthly SLP data were also used to identify the climatological subtropical anticyclones. The same procedure was made using CFSR 6-hourly SLP data in the period 1979–2010.

We use a Monte Carlo method for the estimation of statistical significance in the relationship between intense alongshore wind stress (upper quartile) and migratory anticyclones (Supplementary Fig. 2). One-hundred synthetic time series of randomized samples of the wind stress were performed at each latitude. Then, the probability occurrence of an intense wind stress in the presence of a migratory anticyclone was obtained for each time series. Finally, if the probability of the original wind stress data is larger than the 90th percentile of the randomly generated probability, we consider the relationship between intense wind stress and migratory anticyclone significant.

The position of the STR corresponds to the latitude of maximum SLP in each model and then the model mean is calculated. Longitudes where more than 70% of the models show a poleward shift of the STR in the future are shown in bold.

## DATA AVAILABILITY

The datasets analysed in this study are available on-line. CMIP5 data can be downloaded from <https://esgf-node.llnl.gov/projects/cmip5/> and CFSR data can be downloaded from <https://rda.ucar.edu/pub/cfsr.html>.

## CODE AVAILABILITY

The cyclone tracking software used in this study is freely available and may be obtained by contacting Professor Ian Simmonds from the University of Melbourne ([simmonds@unimelb.edu.au](mailto:simmonds@unimelb.edu.au)).

Received: 18 August 2018; Accepted: 28 October 2019;

Published online: 29 November 2019

## REFERENCES

- Strub, P. T., Combes, V., Shillington, F. A. & Pizarro, O. in *International Geophysics* Vol. 103 (eds Siedler, G. et al.) 339–384 (Academic Press, 2013).
- Capone, D. G. & Hutchins, D. A. Microbial biogeochemistry of coastal upwelling regimes in a changing ocean. *Nat. Geosci.* **6**, 711–717 (2013).
- Croll, D. A. et al. From wind to whales trophic links in a coastal upwelling system. *Mar. Ecol. Prog. Ser.* **289**, 117–130 (2005).
- Brian, A. et al. Upwelling-driven nearshore hypoxia signals ecosystem and oceanographic changes in the northeast Pacific. *Nature* **429**, 749–754 (2004).
- Silva, C. et al. Predicting habitat suitability and geographic distribution of anchovy (*Engraulis ringens*) due to climate change in the coastal areas off Chile. *Prog. Oceanogr.* **146**, 159–174 (2016).
- Wang, D., Gouhier, T. C., Menge, B. A. & Ganguly, A. R. Intensification and spatial homogenization of coastal upwelling under climate change. *Nature* **518**, 390–394 (2015).
- Rykcaczewski, R. R. et al. Poleward displacement of coastal upwelling-favorable winds in the ocean's eastern boundary currents through the 21st century. *Geophys. Res. Lett.* **42**, 6424–6431 (2015).
- Goubanova, K. et al. Statistical downscaling of sea-surface wind over the Peru–Chile upwelling region: diagnosing the impact of climate change from the IPSL-CM4 model. *Clim. Dyn.* **36**, 1365–1378 (2011).
- Garreaud, R. D. & Muñoz, R. C. The low-level jet off the West Coast of Subtropical South America: structure and variability. *Mon. Weather Rev.* **133**, 2246–2261 (2005).
- Aguirre, C., Pizarro, Ó., Strub, P. T., Garreaud, R. & Barth, J. A. Seasonal dynamics of the near-surface alongshore flow off central Chile. *J. Geophys. Res. Oceans* **117**, <https://doi.org/10.1029/2011jc007379> (2012).
- Renault, L., Hall, A. & McWilliams, J. C. Orographic shaping of US West Coast wind profiles during the upwelling season. *Clim. Dyn.* **46**, 273–289 (2016).
- Renault, L. et al. Upwelling response to atmospheric coastal jets off central Chile: a modeling study of the October 2000 event. *J. Geophys. Res. Oceans* **117**, <https://doi.org/10.1029/2011jc007446> (2012).
- Aguirre, C., Garreaud, R. D. & Rutllant, J. A. Surface ocean response to synoptic-scale variability in wind stress and heat fluxes off south-central Chile. *Dyn. Atmospheres Oceans* **65**, 64–85 (2014).
- Adams, K. A., Barth, J. A. & Chan, F. Temporal variability of near-bottom dissolved oxygen during upwelling off central Oregon. *J. Geophys. Res. Oceans* **118**, 4839–4854 (2013).
- Kapsenberg, L. & Hofmann, G. E. Ocean pH time-series and drivers of variability along the northern Channel Islands, California, USA. *Limnol. Oceanogr.* **61**, 953–968 (2016).
- Iles, A. C. et al. Climate-driven trends and ecological implications of event-scale upwelling in the California Current System. *Glob. Chang. Biol.* **18**, 783–796 (2012).
- García-Reyes, M., Largier, J. L. & Sydeman, W. J. Synoptic-scale upwelling indices and predictions of phyto- and zooplankton populations. *Prog. Oceanogr.* **120**, 177–188 (2014).
- Seager, R. et al. Air–sea interaction and the seasonal cycle of the subtropical anticyclones. *J. Clim.* **16**, 1948–1966 (2003).
- Muñoz, R. & Garreaud, R. Dynamics of the low-level jet off the West Coast of Subtropical South America. *Mon. Weather Rev.* **133**, 3661–3677 (2005).
- Rahn, D. A. & Garreaud, R. D. A synoptic climatology of the near-surface wind along the west coast of South America. *Int. J. Climatol.* **34**, 780–792 (2014).
- Pepler, A., Dowdy, A. & Hope, P. A global climatology of surface anticyclones, their variability, associated drivers and long-term trends. *Clim. Dyn.* **52**, 5397–5412 (2019).
- Belmadani, A., Echevin, V., Codron, F., Takahashi, K. & Junquas, C. What dynamics drive future wind scenarios for coastal upwelling off Peru and Chile? *Clim. Dyn.* **43**, 1893–1914 (2013).
- Lu, J., Vecchi, G. A. & Reichler, T. Expansion of the Hadley cell under global warming. *Geophys. Res. Lett.* **34**, <https://doi.org/10.1029/2006gl028443> (2007).
- Li, W. et al. Intensification of the Southern Hemisphere summertime subtropical anticyclones in a warming climate. *Geophys. Res. Lett.* **40**, 5959–5964 (2013).
- Vizy, E. C. & K. Sun, X. Decadal change of the south Atlantic ocean Angola-Benguela frontal zone since 1980. *Clim. Dyn.* **51**, 22 (2018).
- Schneider, W., Donoso, D., Garcés-Vargas, J. & Escribano, R. Water-column cooling and sea surface salinity increase in the upwelling region off central-south Chile driven by a poleward displacement of the South Pacific High. *Prog. Oceanogr.* **151**, 11 (2017).
- Arblaster, J. M., Meehl, G. A. & Karoly, D. J. Future climate change in the Southern Hemisphere: competing effects of ozone and greenhouse gases. *Geophys. Res. Lett.* **38**, <https://doi.org/10.1029/2010gl045384> (2011).
- Zheng, F., Li, J., Clark, R. & Nnamchi, H. Simulation and projection of the Southern Hemisphere annular mode in CMIP5 models. *J. Clim.* **26**, 9860–9879 (2013).
- Chang, E. K. M., Guo, Y. & Xia, X. CMIP5 multimodel ensemble projection of storm track change under global warming. *J. Geophys. Res. Atmos.* **117**, <https://doi.org/10.1029/2012jd018578> (2012).
- Ranjha, R., Svensson, G., Tjernström, M. & Semedo, A. Global distribution and seasonal variability of coastal low-level jets derived from ERA-Interim reanalysis. *Tellus A* **65**, 20412 (2013).
- Burk, S. & a., T. W. The summertime low-level jet and marine boundary layer structure along the California coast. *Mon. Weather Rev.* **124**, 668–685 (1996).
- Nicholson, S. E. A low-level jet along the Benguela coast, an integral part of the Benguela current ecosystem. *Clim. Change* **99**, 613–624 (2009).
- Soares, P. M. M., Cardoso, R. M., Semedo, A., Chinita, M. J. & Ranjha, R. Climatology of the Iberia coastal low-level wind jet: weather research forecasting model high-resolution results. *Tellus A* **66**, <https://doi.org/10.3402/tellusa.v66.2377> (2014).
- Lima, D. C. A., Soares, P. M. M., Semedo, A. & Cardoso, R. M. A global view of coastal low-level wind jets using an ensemble of reanalyses. *J. Clim.* **31**,



- 1525–1546 (2018).
35. Semedo, A. et al. The impact of climate change on the global coastal low-level wind jets: EC-EARTH simulations. *Glob. Planet. Change* **137**, 88–106 (2016).
  36. Soares, P. M. M., Lima, D. C. A., Cardoso, R. M. & Semedo, A. High resolution projections for the western Iberian coastal low level jet in a changing climate. *Clim. Dyn.* **49**, 1547–1566 (2016).
  37. Richter, I. Climate model biases in the eastern tropical oceans: causes, impacts and ways forward. *WIREs Clim. Change* **6**, 13 (2015).
  38. Brady, R. X., Alexander, M. A., Lovenduski, N. S. & Rykaczewski, R. R. Emergent anthropogenic trends in California Current upwelling. *Geophys. Res. Lett.* **44**, 5044–5052 (2017).
  39. García-Reyes, M. et al. Under pressure: climate change, upwelling, and eastern boundary upwelling ecosystems. *Front. Mar. Sci.* **2**, <https://doi.org/10.3389/fmars.2015.00109> (2015).
  40. Saha, S. et al. The NCEP Climate Forecast System Reanalysis. *Bull. Am. Meteorol. Soc.* **91**, 1015–1058 (2010).
  41. Riahi, K. et al. RCP 8.5—A scenario of comparatively high greenhouse gas emissions. *Clim. Change* **109**, 33–57 (2011).
  42. Smith, S. D. Coefficients for sea surface wind stress, heat flux, and wind profiles as a function of wind speed and temperature. *J. Geophys. Res.* **93**, 15467 (1988).
  43. Bravo, L., Ramos, M., Astudillo, O., Dewitte, B. & Goubanova, K. Seasonal variability of the Ekman transport and pumping in the upwelling system off central-northern Chile (~30°S) based on a high-resolution atmospheric regional model (WRF). *Ocean Sci.* **12**, 1049–1065 (2016).
  44. Thompson, S. A. et al. Linking predators to seasonality of upwelling: Using food web indicators and path analysis to infer trophic connections. *Prog Oceanography* **101**, 106–120 (2012).
  45. Simmonds, I. & Keay, K. Mean Southern Hemisphere Extratropical Cyclone Behavior in the 40-Year NCEP–NCAR Reanalysis. *J. Clim.* **13**, 873–885 (2000).
  46. Grieger, J., Leckebusch, G. C., Donat, M. G., Schuster, M. & Ulbrich, U. Southern Hemisphere winter cyclone activity under recent and future climate conditions in multi-model AOGCM simulations. *Int. J. Climatol.* **34**, 3400–3416 (2014).

## ACKNOWLEDGEMENTS

We acknowledge the World Climate Research Programme's Working Group on Coupled Modelling, which is responsible for CMIP5, and we thank the climate modelling groups (listed in Supplementary Table 1) for producing and making available their model outputs. This work was partially funded by FONDAP-CONICYT 15110009. C.A. acknowledges support by Conicyt through PAI program no. 79150062 and Fondecyt grant no. 11171163. M.R. acknowledges support by Fondecyt grant no.

1171773 and D.A.R. acknowledges support by the National Science Foundation grant AGS-1439515.

## AUTHOR CONTRIBUTIONS

Original idea, design, analyses, figures: C.A. Cyclone tracking software, analyses, and figures: M.R. All authors discussed the results and contributed to writing the manuscript.

## COMPETING INTERESTS

The authors declare no competing interests.

## ADDITIONAL INFORMATION

**Supplementary information** is available for this paper at <https://doi.org/10.1038/s41612-019-0101-9>.

**Correspondence** and requests for materials should be addressed to C.A.

**Reprints and permission information** is available at <http://www.nature.com/reprints>

**Publisher's note** Springer Nature remains neutral with regard to jurisdictional claims in published maps and institutional affiliations.



**Open Access** This article is licensed under a Creative Commons Attribution 4.0 International License, which permits use, sharing, adaptation, distribution and reproduction in any medium or format, as long as you give appropriate credit to the original author(s) and the source, provide a link to the Creative Commons license, and indicate if changes were made. The images or other third party material in this article are included in the article's Creative Commons license, unless indicated otherwise in a credit line to the material. If material is not included in the article's Creative Commons license and your intended use is not permitted by statutory regulation or exceeds the permitted use, you will need to obtain permission directly from the copyright holder. To view a copy of this license, visit <http://creativecommons.org/licenses/by/4.0/>.

© The Author(s) 2019